ELSEVIER

Journal of Environmental Management 85 (2007) 563–573

Journal of Environmental Management

www.elsevier.com/locate/jenvman

Net primary productivity of China's terrestrial ecosystems from a process model driven by remote sensing

X. Feng[a,*], G. Liu[a], J.M. Chen[b], M. Chen[b], J. Liu[c], W.M. Ju[b], R. Sun[d], W. Zhou[a]

[a]*State Key Laboratory of Resource and Environmental Information System, IGSNRR, CAS, 11A Datun Road Anwai, Room 2315, Beijing 100101, PR China*
[b]*Department of Geography and Program in Planning, University of Toronto, Toronto, Canada*
[c]*Atmospheric Science, Department of Physics, University of Toronto, Toronto, Canada*
[d]*Department of Resource and Environment Sciences, Beijing Normal University, Beijing, PR China*

Received 21 May 2005; received in revised form 21 September 2006; accepted 25 September 2006
Available online 17 January 2007

Abstract

The terrestrial carbon cycle is one of the foci in global climate change research. Simulating net primary productivity (NPP) of terrestrial ecosystems is important for carbon cycle research. In this study, China's terrestrial NPP was simulated using the Boreal Ecosystem Productivity Simulator (BEPS), a carbon-water coupled process model based on remote sensing inputs. For these purposes, a national-wide database (including leaf area index, land cover, meteorology, vegetation and soil) at a 1 km resolution and a validation database were established. Using these databases and BEPS, daily maps of NPP for the entire China's landmass in 2001 were produced, and gross primary productivity (GPP) and autotrophic respiration (RA) were estimated. Using the simulated results, we explore temporal–spatial patterns of China's terrestrial NPP and the mechanisms of its responses to various environmental factors. The total NPP and mean NPP of China's landmass were 2.235 GtC and 235.2 gC m^{-2} yr^{-1}, respectively; the total GPP and mean GPP were 4.418 GtC and 465 gC m^{-2} yr^{-1}; and the total RA and mean RA were 2.227 GtC and 234 gC m^{-2} yr^{-1}, respectively. On average, NPP was 50.6% of GPP. In addition, statistical analysis of NPP of different land cover types was conducted, and spatiotemporal patterns of NPP were investigated. The response of NPP to changes in some key factors such as LAI, precipitation, temperature, solar radiation, VPD and AWC are evaluated and discussed.

Keywords: BEPS; Net primary productivity (NPP); Leaf area index (LAI); Land cover; Soil available water capacity (AWC)

1. Introduction

Terrestrial carbon and water cycles are important foci in global climate change research. A key component of the terrestrial carbon cycle is net primary productivity (NPP), defined as the difference between accumulated photosynthesis and accumulated autotrophic respiration by green plants per unit time and space (Lieth and Whittaker, 1975). NPP is equivalent to the net amount of carbon added to plant biomass per unit of space and time (Chen et al., 1999). Productivity is fundamental to ecology, and carbon storage by land ecosystems can play an important role in limiting the rate of atmospheric CO_2 increase. NPP data are useful in many applications (Bonan, 1995; Hunt et al., 1996; Chen et al., 2000); and they are increasingly relevant to land use policies. There are two challenges in using a model to estimate NPP accurately: (1) the mechanisms for simulating carbon cycle processes should represent our latest understanding of ecosystem functioning and (2) the model should have the capacity to use as many as possible relevant datasets for input (Bunkei and Masayuki, 2002).

Ruimy suggested three types of models which are generally used to estimate terrestrial NPP (Ruimy et al., 1999). They are: (1) statistical models (Lieth and Whittaker, 1975), (2) parametric models (Potter et al., 1993; Prince, 1995; Ruimy et al., 1999), and (3) process models (Running et al., 1989; Foley, 1995; Mellio et al., 1993;

*Corresponding author. Tel.: +86 10 64889042 2; fax: +86 10 64889630.
E-mail addresses: fengxf@lreis.ac.cn, xianfeng_feng@hotmail.com (X. Feng).

0301-4797/$ - see front matter © 2006 Elsevier Ltd. All rights reserved.
doi:10.1016/j.jenvman.2006.09.021

Bonan, 1995; Liu et al., 1997). The first- and second-type models are simple and easy to use, but they lack the strong theory and understanding of ecosystem function. Process models generally incorporate mechanisms to simulate various plant physiological processes including photosynthesis, autotrophic respiration and transpiration, and therefore potentially produce more reliable results than other types of models. However, process models' use is hampered by data availability and computing resources. Another challenge is the need for temporal and spatial scaling, because most process models have been developed and tested at the stand level (Chen et al., 1999). Given computing resources, modelers often have to make trade-offs between spatial resolution and model execution time steps. Remote sensing data provide important spatially explicit inputs for process models. These include vegetation indices to derive the key driving variables and land cover types to reflect substantial physiological differences among vegetation types (Running et al., 1989; Hunt et al., 1996; Sellers et al., 1996; Liu et al., 1997; Bonan, 1993).

The objectives of this study were (i) to simulate China's terrestrial NPP using a process model based on remote sensing data at a 1-km spatial resolution, (ii) to explore spatiotemporal patterns of China's terrestrial NPP, and (iii) to investigate the sensitivity of NPP to various environmental factors. For these purposes, BEPS model parameters were adjusted to China's diverse ecosystems, and a nation-wide spatial database at 1 km resolution was established.

2. Model and data description

China has a vast territory, a variable topography, and a rich variety of ecosystems. The country has a north-south gradient in temperature and an east-west gradient in precipitation driven by the summer monsoon (Hou, 1983; Fullen and Mitchell, 1994; Menzies, 1996). The terrestrial ecosystems include forest, grassland, desert, wetland and cropland. The natural ecosystems range from forest, through grassland, to desert from the east to the west, and forest ecosystems vary along a north- south gradient from boreal forests, through cold- and warm-temperate deciduous forests, to mixed evergreen and deciduous subtropical forests, to evergreen tropical forests (Hou, 1983; Houghton and Hackler, 2003). Agricultural ecosystems are interspersed among other ecosystems. This spatial distribution of terrestrial ecosystems made the simulation of NPP of China more difficult than for the boreal ecosystems of Canada where the BEPS model was originally developed.

2.1. Description of the model

Boreal ecosystem productivity simulator (BEPS) was used to estimate NPP across China's landmass (Liu et al., 1997; Chen et al., 1999). The model includes an advanced canopy radiation sub-model to quantify the effects of canopy architecture on the radiation distribution and photosynthesis in the canopy. The photosynthesis sub-model is based on the Farquhar's model scaled to the canopy using a sunlit and shaded leaf stratification approach (Farquhar et al., 1980; Farquhar and Sharkey, 1982). In this study, BEPS was executed at daily time steps for each pixel and the annual NPP was obtained as the sum of daily NPP values. BEPS model parameters were also adjusted for the various ecosystems in China (Table 1), using results of previous studies (Hunt et al., 1996; Liu et al., 1997; Kimball et al., 1997; Foley, 1995).

2.2. Spatially explicit input data

The required BEPS input data, including land cover, LAI, available soil water-holding capacity (AWC), soil water content, DEM and daily meteorological data, were all processed in the same coordinate system (Albers conical equal-area projection). At 1 km resolution, the image size was 5300×4300 pixels.

2.2.1. LAI data

LAI is a key parameter in BEPS for simulating various physical and biological processes including radiation interception, precipitation interception, evaporation from wet leaf surfaces, transpiration, photosynthesis, autotrophic respiration, and others. It was generated from processing and validation of 8-day MODIS image composites derived using the NDVI-LAI algorithm (MODIS-15 product). The LAI data compared favorably against two experimental sites in northeast and northwest China (Liu et al., 2006). In BEPS, a forest cover is treated in two layers, overstorey and understorey, and an empirical relationship between the overstorey LAI (MOD 15) and the understorey LAI was used (Liu et al., 2003).

2.2.2. Land cover data

In BEPS, land cover information is used to specify plant physiological parameters that differ among cover types. The land cover map of China in 2001 was derived from a nation-wide land use map (30 m resolution, interpreted

Table 1
Major vegetation parameters for different land cover types

Land cover	MSC ($mm\,s^{-1}$)	FCI (Ω)	SLA ($m^2\,kg\,C^{-1}$)
DN forest	4.5	0.5	30
EN forest	2.2	0.5	25
DB forest	4	0.7	25
EB forest	6	0.7	20
MF (EN and DB)	4.5	0.6	20
MF (DB and EB)	5	0.7	27
Crop/natural plant	4.5	0.7	20
DS	4	0.6	10
ES	4	0.6	10
Forest/grass	3	0.7	20
Grass land	5	0.9	30
Crop land	5	0.9	30

Detail information about land cover type in Table 2.

from Landsat TM images) and a vegetation map (scale 1:2.5 million, vector format). As in the land use map (aggregated to 1 km resolution), no forest type information was given, the vegetation map with different forest types was used to separate the generally forest class in the land use map into several forest types. Table 2 shows the class and code of the land cover data. To obtain the final land cover distribution for use in BEPS (high spatial resolution and fine classification), the land use and vegetation data were fused as follows (Fig. 1):

Step 1. Each class in the vegetation map was matched with a relevant class in land use data.

Step 2: The vegetation map was resampled with the same spatial resolution as the land use map.

Step 3: Each forest pixel in the land use map was assigned a forest type based on the vegetation map using the cell-to-cell function in ArcGIS. As the locations of forest pixels in these two maps do not often match exactly, a nearest neighbor principle was followed, as such that a forest pixel in the land use map based on remote sensing is taken as accurate while the its forest type is determined by the nearest forest of a known type in the vegetation map.

This new land cover map processed in this way was validated based on site data, MODIS-15 data and land cover product from VEGETATION (provided by Institute of Remote Applications of Chinese Academy of Sciences). In this manner, the final land cover of China in 2001 with a resolution of 1 km was obtained (Fig. 2).

Table 2
The class name and code of land cover data

Code	Class name
1	Deciduous needle leaf forest (DN)
2	Evergreen needle leaf forest in temperate zone (EN-N)
3	Evergreen needle leaf forest in tropic zone and subtropics zone (EN-S)
4	Deciduous broadleaf forest (DB)
5	Evergreen broadleaf forest (EB)
6	Mixed forest: EN and DB (MF)
7	Mixed broadleaf forest :DB and EB (MF)
8	Crop/natural plant
9	Deciduous shrub (DS)
10	Evergreen shrub (ES)
11	Forest/grass
12	Grass land
13	Paddy (crop land)
14	Dry land (crop land)
15	Water
16	Ice and snow
17	Resident and built-up land
18	Barren or sparse vegetation

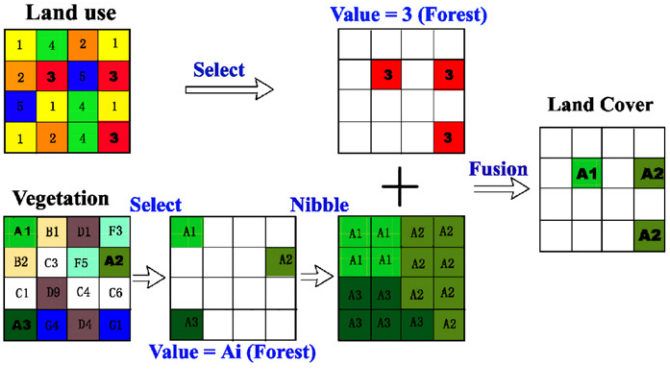

Fig. 1. Flow chart of fusion using land use data and vegetation data. Class 3 in the land use map in this case is forest, while classes Ai in the vegetation map are also forest. The final locations of forests are based on the land use map.

2.2.3. Soil data

The amount of available soil water is one of the most important factors affecting plant growth. Soil available water capacity (AWC) is determined primarily by soil texture. An AWC map was produced based on the relation between soil texture and AWC classes as shown in Table 3 (Jong et al., 1984; Wenzuo et al., 2005). The resulting China-wide AWC map is shown in Fig. 3.

2.2.4. Meteorological data

Algorithm for interpolating meteorological data. Meteorological data of 680 stations were interpolated to individual 1-km pixels using ANUSPLINE (Hutchinson, 1991, 1995, 1998, 2002). Daily meteorological data were interpolated using thin plate smoothing splines based on topography. The daily meteorological data include radiation, maximum and minimum temperature, mean humidity and total precipitation, and snowpack data at the beginning of a year.

AUSPLIN is a suite of FORTRAN programs that has been applied successfully at regional scales (Price et al., 2000). There are three independent spline variables: longitude, latitude and elevation above sea-level. A general model for a thin plate spline function f fitted to n data values Z_i at positions X_i is given by (Hutchinson, 1995)

$$Z_i = f(x_i) + \varepsilon_i, \quad i = 1, \ldots, n, \tag{1}$$

where X_i typically represents longitude, latitude, and suitably scaled elevation; and ε_i are random errors with zero means which account for measurement errors as well as deficiencies in the spline model, such as local effects below the resolution of the data network. Compared with other interpolation methods such as ANSPLIN, GIDS, Surfer and ARC GRID, ANUSPLIN was generally more accurate in interpolating meteorological variables (Price et al., 2000; Feng, 2004), so ANSPLIN was selected in this study. Fig. 4 shows a DEM map of China, a critical input to the interpolation model.

Because radiation observation stations were very sparse (only 98 stations), the daily global radiation fields from the National Center for Environmental Prediction (NCEP) of the USA were used for modeling. Since the NCEP data were found to be positively biased compared with the existing observations, we used the observed global radiation data from the 98 stations to

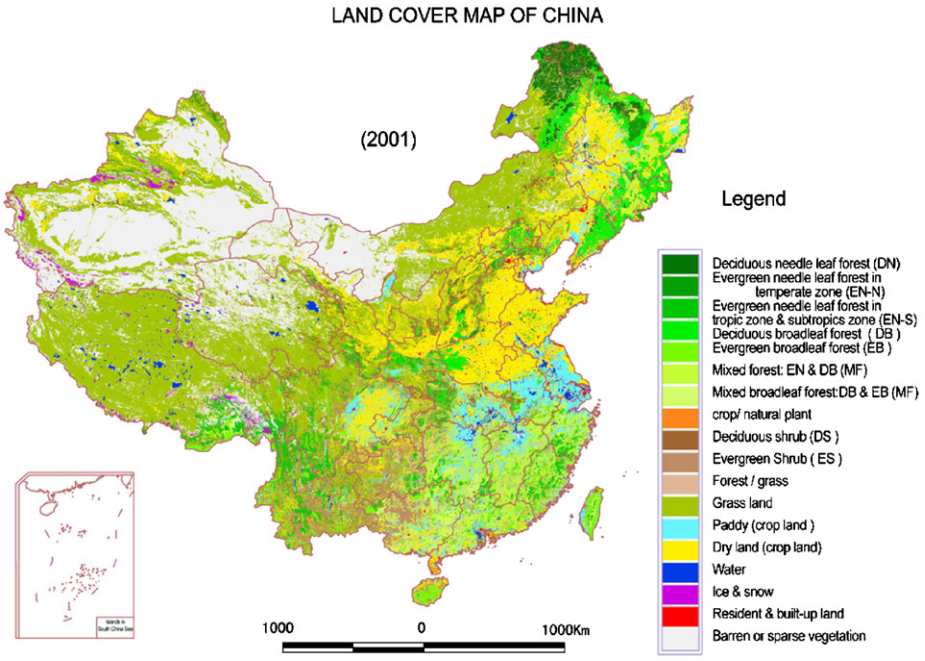

Fig. 2. Land cover map of China derived from data fusion.

Table 3
The relationship between soil available water capacity (AWC) and soil texture

Class	AWC (mm)	Texture group
0	—	Soil with a high water table
1	50	Sand; loamy sand
2	100	Sandy loam; gravelly loam
3	150	Very fine sandy loam; loam; gravelly silt loam
4	200	Silt loam; sandy clay loam; clay loam
5	250	Silty clay loam; sandy clay; silty clay; clay; heavy clay
6	—	Solonetzic soils

correct the NCEP data:

$$\text{Observation radiation} = A \times \text{NCEP}, \quad (2)$$

where A is the coefficient between the observed radiation and NCEP at every station. By regression analysis, A was found to vary between 0.5415 and 0.8514 at different stations, the majority ranging from 0.68 to 0.75. Using the average A of 0.718. Eq. (3) was employed to obtain the final radiation value for each 1 km pixel.

$$\text{Observation radiation} = 0.718 \times \text{NCEP}. \quad (3)$$

2.2.5. Forest biomass data

Biomass is a critical parameter for calculating autotrophic respiration. In this study, forest biomass data were generated using non-linear relationships between biomass and LAI (Bonan, 1995; Hunt et al., 1996; Liu et al., 1999; Feng, 2000):

$$B = AX + BX^2, \quad (4)$$

where B is aboveground biomass in $\mathrm{kg\,m^{-2}}$ and A and B are cover-type dependent parameters. The root biomass was estimated through correlation with the aboveground biomass according to the R/T of each forest type (R/T means root top ratio). After validation against ground data (Luo, 1996; Feng et al., 1999), a total forest biomass map of China in 2001 was produced (Fig. 5). This total biomass is separated into root, leaf and stem components in calculating autotrophic respiration. Table 4 shows some validation results, just for example boreal/alpine *picea-abies* forest. As a whole, the bias of simulating biomass was found to vary between +18.3% and −24.2% at different sites and plots, the majority ranging from +10.7% to −14.8%. This biomass simulation can be improved through considering tree age in the empirical biomass equations and separating mixed pixels into areal fractions of deciduous and conifer cover types.

3. Results and discussion

3.1. Validation of the NPP map

The NPP map was compared with simulated high resolution NPP values based on the field data from four sites (Changbaishan, Heihe, Xingguo, Liping). Table 5 shows the comparison of MODIS-NPP (modeled NPP using LAI data derived from the MODIS product, pixel size 1 km × 1 km) with TM-NPP (modeled NPP using LAI derived from TM data based on the measured data, pixel size 30 m × 30 m) at the Changbaishan site.

Modeled MODIS-NPP for four cover types (MF, EN-N, tundra, cropland) was compared with modeled TM-NPP. Because the spatial resolution was very different between

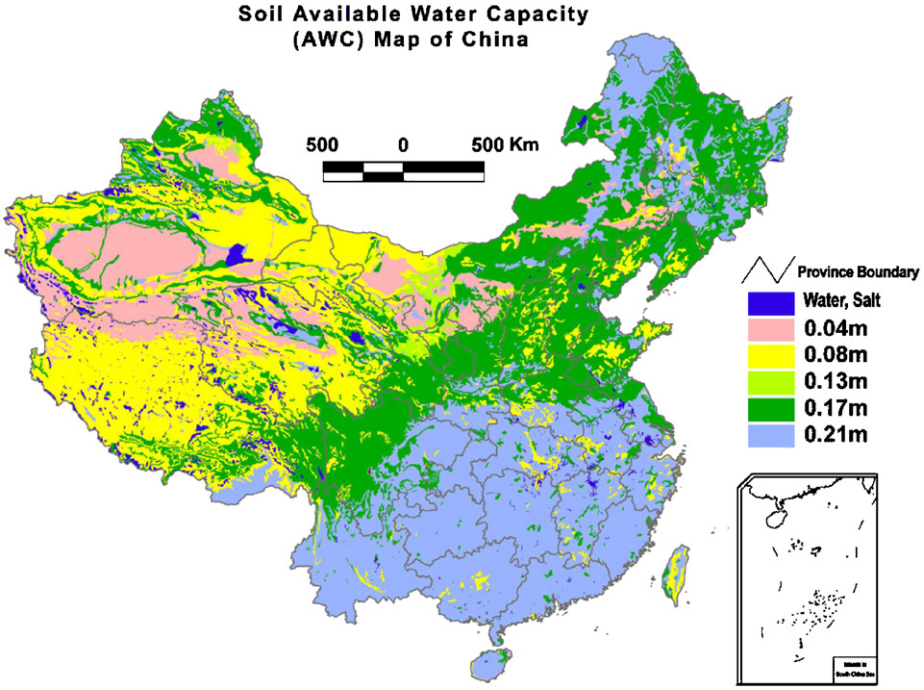

Fig. 3. Available water-holding capacity map of China.

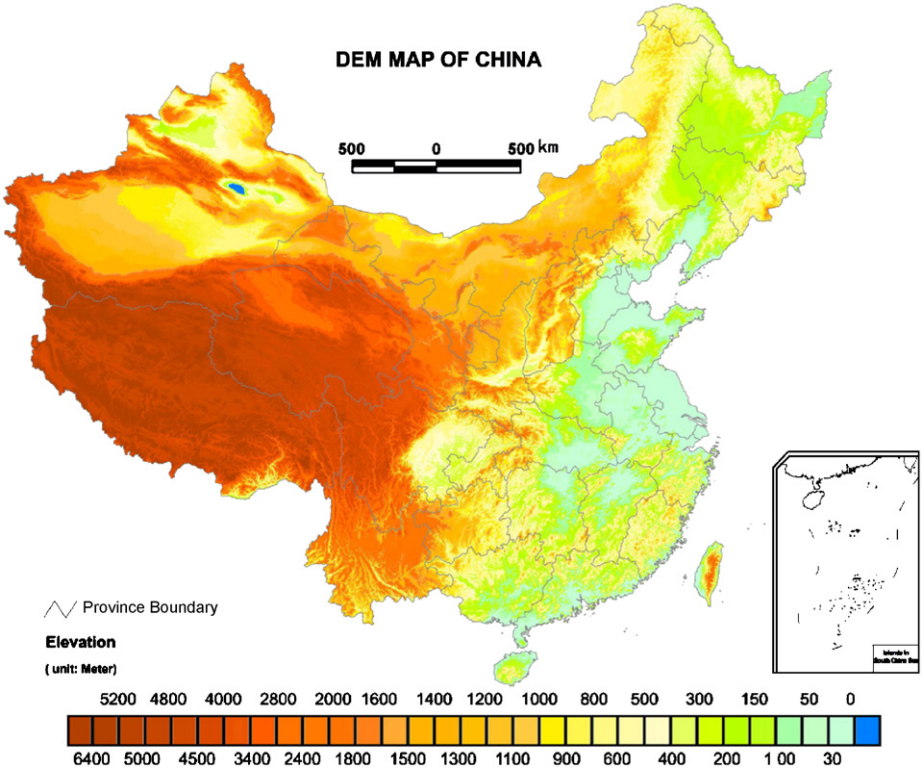

Fig. 4. Digital elevation model (DEM) map of China.

modeled MODIS-NPP and TM-NPP, the comparison based on land cover type was more reasonable than that based on pixels. For deciduous broadleaf forest, the modeled MODIS-NPP is somewhat higher than the modeled TM-NPP. The differences in spatial scales and in LAI are the major factors contributing to differences in NPP. Then the MODIS-NPP was compared with existing ground data in different periods in various locations in China (including every forest type, more than 1000 sites, from 1970 to 1999) (Luo, 1996; Feng et al., 1999). Table 6

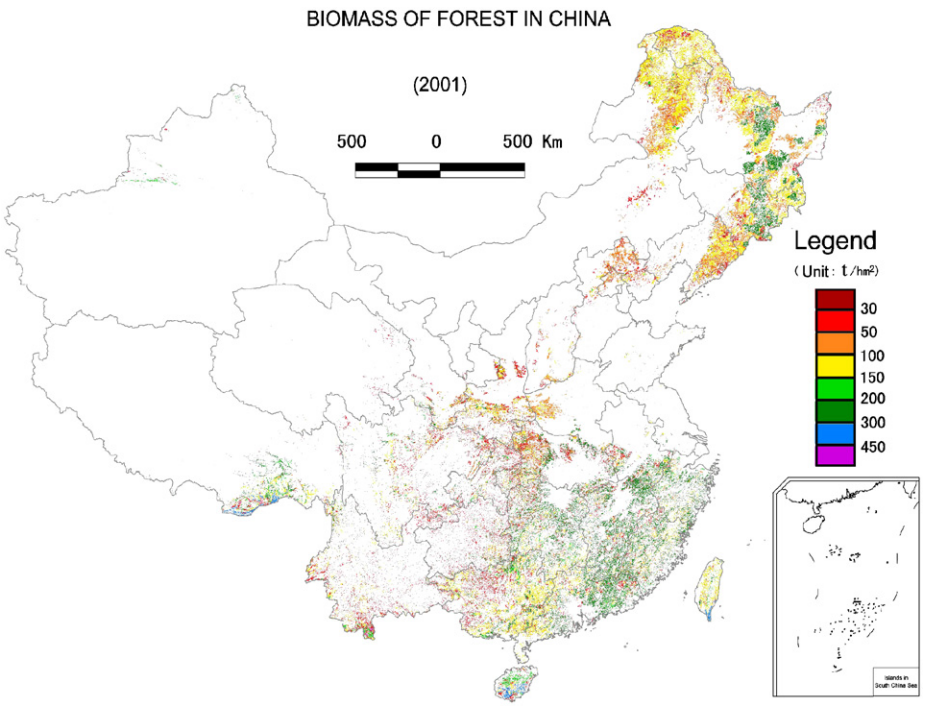

Fig. 5. Forest biomass map of China.

Table 4
Comparison of ground data of biomass and simulated biomass for boreal/alpine *Picea abies* forest (Unit: t DM/hm^2)

Plot no.	Alt. (m)	Lon. (°)	Lat. (°)	Biomass (t DM ha^{-1})	Simulated biomass
3397	3280	103.50	34.60	174.29	150.50
4308	1536	117.20	42.40	80.94	75.80
2368	508	131.80	46.50	104.50	112.40
3314	1017	129.40	44.30	164.32	155.70
2392	950	124.20	52.60	109.88	122.30
4807	2384	105.90	38.77	78.97	75.80
1075	2415	111.83	38.73	134.77	144.50
1067	2276	111.93	38.79	60.54	54.60
1063	2243	112.03	38.89	60.40	58.40
1892	3075	103.00	28.80	562.53	465.30
3335	3500	102.20	31.80	359.56	423.50

shows validation results for subtropical evergreen broadleaf forests. Overall, the modeled MODIS-NPP is very close to the measured data, as many factors (tree age, climate, topography, modeling scale) could have influenced the accuracy of the simulated NPP.

3.2. Annual NPP

The NPP map of China in 2001 is shown in Fig. 6 (pixel size 1 km × 1 km), and the corresponding gross primary productivity (GPP) and autotrophic respiration (AR) maps are shown in Fig. 7 and Fig. 8, respectively. Excluding open water bodies (the NPP of these areas is set to 0 according to the land cover map), the average NPP and total NPP over China in 2001 were 235.2 gC m^{-2} yr^{-1} and 2.235 GtC, respectively. The mean GPP and total GPP were 465 gC m^{-2} yr^{-1} and 4.418 GtC respectively. The mean AR and total AR were 234 gC m^{-2} yr^{-1} and 2.227 GtC, respectively. On average, NPP was 50.6% of GPP.

Table 5
Comparison of MODIS-NPP with TM-NPP at the Changbaishan site (unit: gC m^{-2} yr^{-1})

Land cover	TM-NPP	Land cover	MODIS-NPP
MF	532	MF	579
DB-1[a]	481	DB	631
DB-2[a]	375		
DB(1 + 2)	467.7		
EN-N	469	EN-N	450
Sparse veg.[a]	138	Sparse veg.	152
Crop	205	Crop	230
Average	462.5	Average	538.4

[a]DB-1 = general DB; DB-2 = mountain birch; Sparse vegetation = Tundra.

3.3. Spatial pattern of China's terrestrial NPP

The spatial distribution of NPP was associated with the land cover and climate factors. Statistical analysis for NPP by land cover shows that high NPP values occurred in forested areas, especially in the tropical and subtropical forest areas with warm climate and sufficient precipitation and radiation. The highest NPP (over 1000 gC m^{-2} yr^{-1}) appeared in southern forested areas, such as Yunan province and Hainan province. Low NPP values were

Table 6
Comparison of simulation NPP with measured NPP at each sample for subtropical evergreen broadleaved forest

Sample accounts	Province	Longitude (°, E)	Latitude (°, N)	Measured NPP ($gC\,m^{-2}\,yr^{-1}$)	Simulation NPP ($gC\,m^{-2}\,yr^{-1}$)
16	Fujian	116.30–119.30	24.70–27.60	897–1621.5	696.3–1224.6
5	Guangdong	110.00–115.60	20.70–24.90	1050.5–1566	984.7–1301.0
21	Guangxi	104.41–110.82	21.85–26.00	503–1464	481.9–1235.3
83	Guizhou	104.57–109.40	24.75–29.22	403.5–1562.5	376.9–1369.0
46	Hunan	109.51–114.15	24.70–29.78	728–1614.5	673.0–1184.2
6	Jiangxi	114.40–114.70	26.50–28.40	966–1659.5	620.1–1273.4
3	Sichuan	103.40–106.39	28.30–28.80	642–1088.5	579.8–943.7
5	Xizang	85.20–97.40	27.90–30.20	644–808	532.1–694.5
31	Yunan	98.78–101.19	23.20–28.75	364–1660.5	286.4–1425.3
2	Zheiang	119.27–120.17	29.48–30.25	728.5–954.5	436.0–891.8

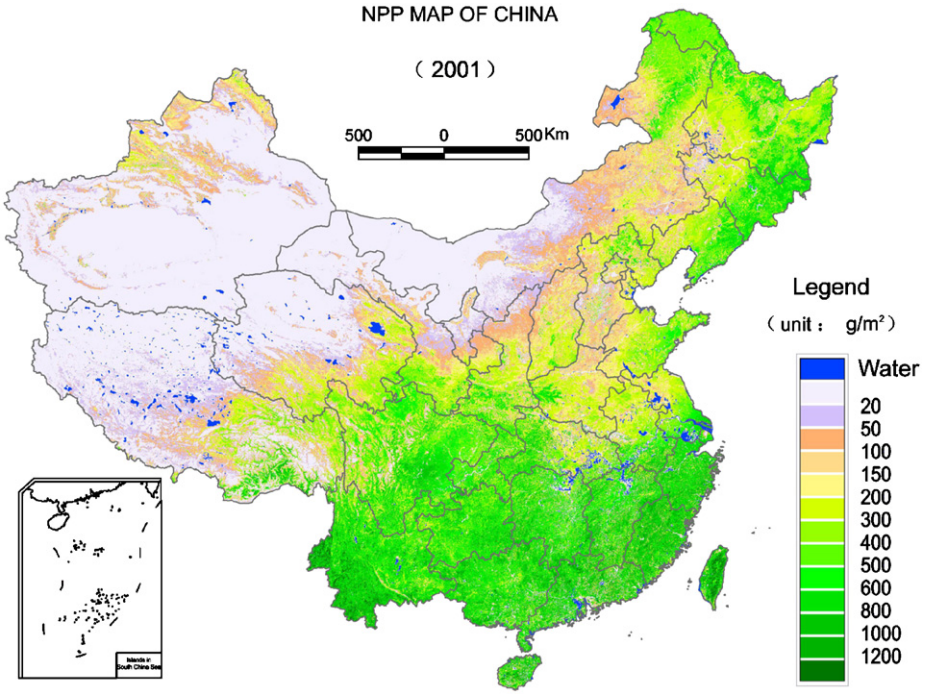

Fig. 6. Net primary productivity (NPP) map of China in 2001.

associated with areas partially covered by snow, ice, bare soil and rock that were located mainly in the northwest China under cold climate with low precipitation and/or low radiation. The lowest NPP values with sparse vegetation appeared in Qinghai province and Gansu province. Statistical results showed the following spatial patterns of China's terrestrial NPP:

1. NPP by land cover per unit area: The simulated NPP values varied greatly with vegetation type and vegetation density (Table 7). Averaged for China, evergreen broadleaf forests ($740.1\,gC\,m^{-2}\,yr^{-1}$) and mixed broadleaf forests ($718.5\,gC\,m^{-2}\,yr^{-1}$) absorbed the most carbon per unit area, followed by mixed forests (broadleaf and needleleaf, $559.5\,gC\,m^{-2}\,yr^{-1}$), needleleaf forests ($456.8\,gC\,m^{-2}\,yr^{-1}$), shrubs ($363.1\,gC\,m^{-2}\,yr^{-1}$), crops ($341.9\,gC\,m^{-2}\,yr^{-1}$), and grasses ($122.6\,gC\,m^{-2}\,yr^{-1}$). Mean NPP values in barren or sparsely covered areas were much smaller ($14.3\,gC\,m^{-2}\,yr^{-1}$).
2. NPP by climate zone per unit area: The simulated NPP values varied with climate zones, because vegetation type and vegetation density are closely related to climate. Averaged for China, the dependence is as follows: tropical forests ($648.5\,gC\,m^{-2}\,yr^{-1}$) > subtropical forests ($637.0\,gC\,m^{-2}\,yr^{-1}$) > temperate forests ($436.3\,gC\,m^{-2}\,yr^{-1}$) > warm temperate forests ($407.4\,gC\,m^{-2}\,yr^{-1}$) > cold temperate forests ($315.2\,gC\,m^{-2}\,yr^{-1}$).

3.4. Temporal pattern of China's terrestrial NPP

The temporal pattern of NPP is evident in the seasonal variation, especially monthly and ten-day NPP distributions.

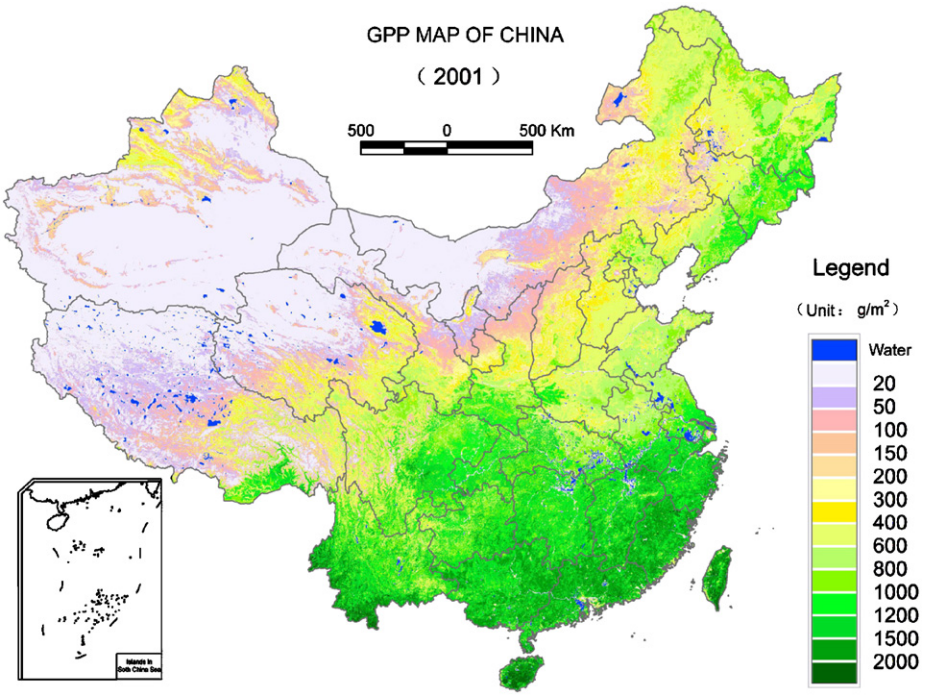

Fig. 7. Gross primary productivity (GPP) map of China in 2001.

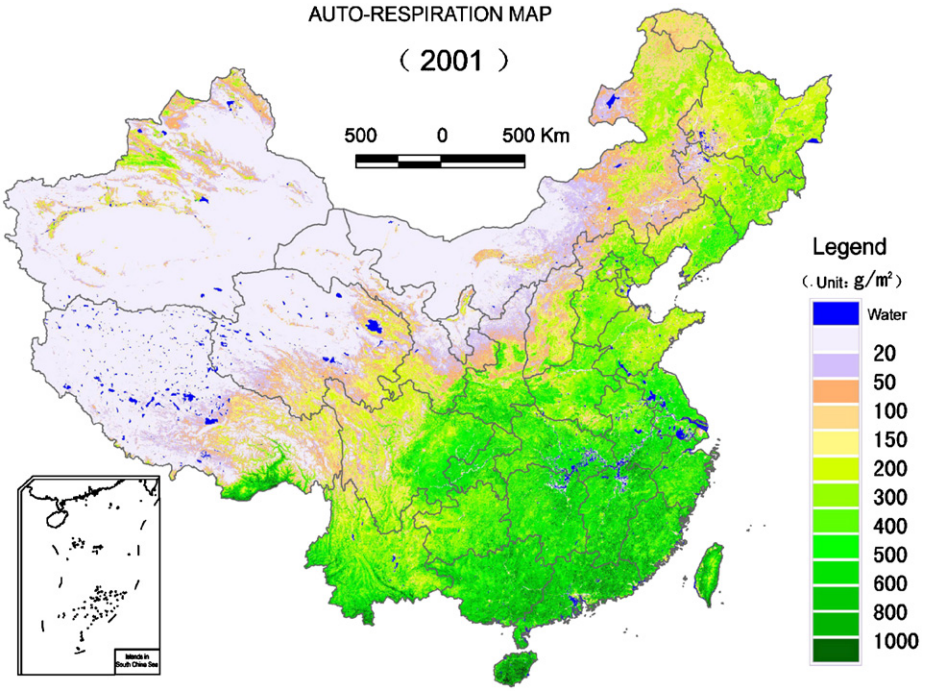

Fig. 8. Autotrophic respiration map of China in 2001.

The monthly NPP distributions in China in 2001 are illustrated in Fig. 9. Modeled results show that the largest NPP occurred between April and October, and especially May to September in 2001. Because of the various climatic zones and vegetation distributions, the NPP temporal patterns varied greatly on a regional basis, from east to west as well as from north to south. The positive NPP values were found during spring, summer and autumn. In some areas, NPP appeared to be slightly negative in the first and last 3 months of the year, indicating that the autotrophic respiration exceeded GPP during these periods. Fig. 10 shows the seasonal variation of average NPP in 10-day intervals in 2001, with a bimodal pattern because of the contribution of double cropping areas as well as mid-summer droughts in some cases. The seasonal distribution patterns also differed significantly among land cover types.

3.5. Sensitivity analysis

Although the BEPS model successfully captured major characteristics of the NPP distribution across China, there are uncertainties arising from various sources. Since the simulated NPP depended greatly on the quality of input data, deficiencies in input data will affect the accuracy of the NPP results. Using sensitivity tests, the influence of uncertainties in the input variables on NPP were identified (Table 8); in each test, one variable was changed while all other variables were kept unchanged. It is evident that the accuracy of LAI has a considerable impact on NPP estimation. On the other hand, the impact of meteorological variables varies depending on the region, season and other conditions.

Table 7
Area, average NPP, and annual NPP of different land cover type

Land cover type	Area (km^2)	Avg. NPP ($gC\,m^{-2}\,yr^{-1}$)	Total NPP ($10^6\,tC$)
Forest land	1,672,625	551.7	922
Needle-leaf	475,331	456.8	215
Deciduous	123,626	421.9	52
Evergreen	351,705	469	165
Broad-leaf	670,393	613.1	410
Deciduous	338,443	499.1	169
Evergreen	173,415	740.1	127
Mixed	158,535	718.5	114
Mixed	526,901	559.5	295
Shrub land	617,514	363.1	224
Deciduous	337,019	252.8	85
Evergreen	280,495	495.5	139
Grass land	2,915,546	122.6	357
Crop land	1,825,517	341.9	624
Dry-land	1,382,429	295.6	409
Paddy	443,088	421.9	215
Mosaic	195,846	356.1	70
Forest/grass	156,845	336.2	53
Crop/natural plant	39,001	436.2	17
Barren	2,044,530	14.3	26
Water	108,356	—	—
Snow and Ice	67,199	—	—
Urban and built-up	55,719	—	—
Other	87,008	—	—
Total	9,589,860	235.2	2235

3.6. Limitations and further work

There are two major limitations of the NPP results presented here in addition to input data limitations. First, the Farquhar's leaf-level photosynthesis model is applied to the canopy in conjunction with improved spatial and temporal scaling schemes. However the model is not adequate for C4 plants, which include some grasses and crops. Second, management effects on plant growth such as

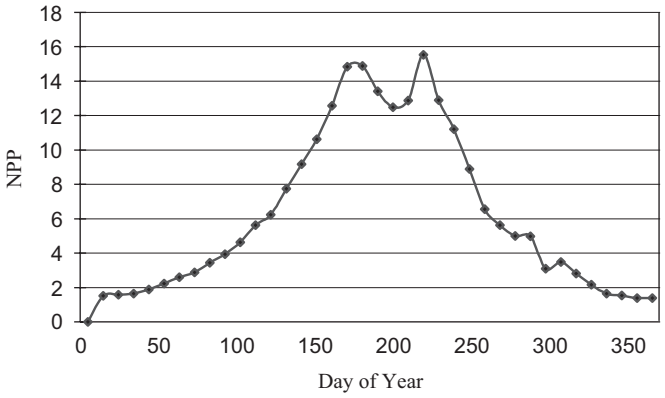

Fig. 10. Seasonal variation of net primary productivity (NPP) in China's terrestrial ecosystems in 2001 (Unit: $gC\,m^{-2}$ in 10 days).

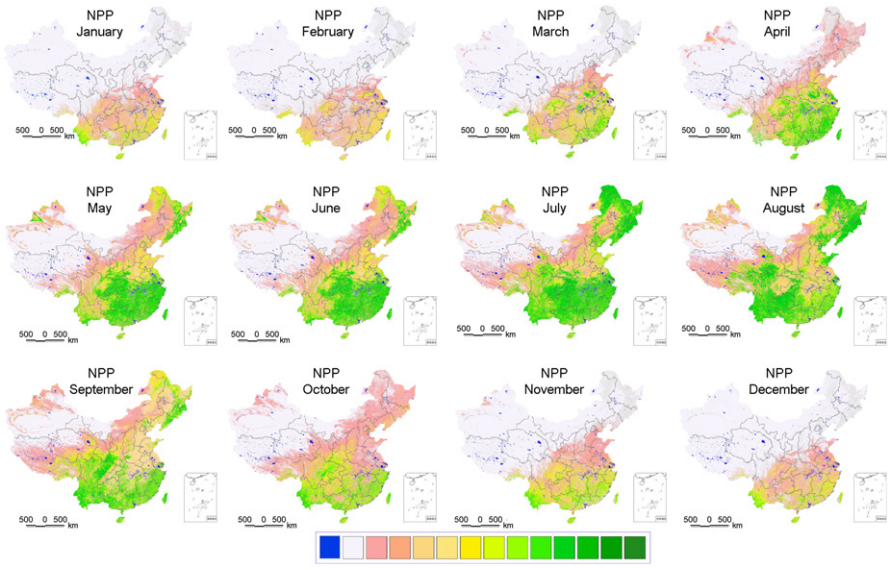

Fig. 9. Monthly variation of NPP in China, 2001.

Table 8
Sensitivity analysis on input data and parameters in the model

Variable	Test range		Effect on National NPP (%)	
	High	Low	High	Low
AWC	20 mm	20 mm	2.856	−2.299
LAI	20%	20%	8.445	−5.100
Precipitation	20%	20%	5.503	−9.043
Radiation	20%	20%	−4.33	3.53
Temperature	1 °C	1 °C	−3.673	2.147
VPD	20%	20%	5.124	−6.112

irrigation, insect control, and fertilizer application, have not been considered in the modeling. These limitations can be overcome, once more spatially explicit data become available.

4. Conclusion

A model for simulating NPP of China's terrestrial ecosystems has been adapted, tested, and used to simulate NPP distribution over China's landmass at 1 km resolution using input data derived from remote sensing and other sources at 8-day intervals for the year 2001. The total NPP and mean NPP of China's landmass in 2001 were 2.235 GtC and 235.2 $gC\,m^{-2}\,yr^{-1}$, respectively. Through model sensitivity tests, LAI was found to have the largest effect on NPP estimation. Meteorological variables had highly variable effects on NPP estimation depending on region, season and vegetation type.

Acknowledgements

The authors are grateful to NASA for MODIS data and NCEP/NCAR CDC for radiation data. This study is part of a Sino-Canada cooperation project supported by the Canadian International Development Agency and the Chinese Academy of Sciences.

References

Bonan, G.B., 1993. Importance of leaf area index and forest type when estimating photosynthesis in boreal forests. Remote Sensing of Environment 43, 303–314.

Bonan, G.B., 1995. Land-atmosphere CO2 exchange simulated by a land surface process model coupled to an atmospheric general circulation model. Journal of Geographysical Research 100 (D2), 2817–2831.

Bunkei, M., Masayuki, T., 2002. Integrating remotely sensed data with an ecosystem model to estimate net primary productivity in East Asia. Remote Sensing of Environment 81, 58–66.

Chen, J.M., Liu, J., Cihlar, J., et al., 1999. Daily canopy photosynthesis model through temporal and spatial scaling for remote sensing alications. Ecological Modelling 124, 99–199.

Chen, J.M., Chen, W., Liu, J., Cihlar, J., 2000. Carbon budget of boreal forests estimated from the change in disturbance, climate, nitrogen and CO2: results for Canada in 1985–1996. Global Biogeochemical Cycle 14, 839–850.

Farquhar, G.D., Sharkey, T.D., 1982. Stomatal conductance and photosynthesis. Annual Review of Plant Physiology 33, 317–345.

Farquhar, G.D., von Caemmerer, S., Berry, J.A., 1980. A biochemical model of photosynthetic CO_2 assimilation in leaves of C3 species. Planta 149, 78–90.

Feng, X., 2000. Study on Dynamic Monitoring of Terrestrial Biomass Using Remote Sensing in China Based on GIS, Master D. dissertation, Shaanxi Normal University, Xi'an.

Feng, X., 2004. Simulating net primary productivity and evaportranspiration of terrestrial ecosystems in China using a process model driven by remote sensing. Ph.D. Disseration, Institue of geographical science and Natural Resource Research of CAS, Beijing.

Feng, Z., Wang, X., Wu, G., 1999. Biomass and productivity offorest ecosystems in China. Science Press, Beijing.

Foley, J.A., 1995. An equilibrium model of the terrestrial carbon budget. Tellus 47B, 310–319.

Fullen, M.A., Mitchell, D.J., 1994. Desertification and reclamation in northcentral China. AMBIO 23, 131–135.

Hou, X.Y., 1983. Vegetation of China with reference to its geographical distribution. Annals of the Missouri Botanical Garden 70, 508–548.

Houghton, R.A., Hackler, J.L., 2003. Sources and sinks of carbon from land-use change in China. Global Biogeochemical Cycles 17 (2), 1034.

Hunt, J.E.R., Piper, S.C., Nemani, R., et al., 1996. Global net carbon exchange and intra-annual atmospheric CO2 concentrations predicted by and ecosystem process model and three-dimensional atmospheric transport model. Global Biogeochemical Cycles 10, 431–456.

Hutchinson, M.F., 1991. The alication of thin-plate smoothing splines to continent-wide data assimilation. In: Jasper, J.D. (Ed.), Data assimilation systems. BMRC Res. Report No. 27, Bureau of Meteorology, Molbourne, pp. 104–113.

Hutchinson, M.F., 1995. Interpolating mean rainfall using thin plate smoothing splines. International Journal of GIS 9, 305–403.

Hutchinson, M.F., 1998. Interpolation of rainfall data with thin plate smoothing splines—I: two dimensional smoothing of data with short range correlation. Journal of Geographic Information and Decision Analysis 2, 152–167.

Hutchinson, M.F., 2002. ANUSPLIN Version 4.2 User Guide.

Jong, R.De., Shields, J.A., Sly, W.K., 1984. Estimated soil water reserves applicable to a wheat-fallow rotation for generalized soil areas mapped in southern Saskatchewan. Canadian Journal of Soil Science 64, 667–680.

Kimball, J.S., Thornton, P.E., White, M.A., et al., 1997. Simulation forest productivity and surface-atmosphere carbon exchange in the BOREAS study region. Tree Physiology 17, 589–599.

Lieth, H., Whittaker, R.H. (Eds.), 1975. Primary Productivity of the Biosphere. Speinger, New York.

Liu, J., Chen, J.M., Cihlar, J., Park, W.M., 1997. A process-based boreal ecosystem productivity simulator using remote sensing inputs. Remote Sensing of Environment 62, 158–175.

Liu, J., Chen, J.M., Cihlar, et al., 1999. Net primary productivity distribution in the BOREAS region from a process model using satellite and surface data. Journal of Geophysical Research 104 (22), 27735–27754.

Liu, J., Chen, J.M., Cihlar, J., 2003. Mapping evapotranspiration based on remote sensing: an application to canada's landmass. Water Resources Research 39, 1189–1200.

Liu, R., Chen, J.M., Liu, J., Deng, F., Sun, R. Application of a new leaf area index algorithm to China's landmass using MODIS data for carbon cycle research. Journal of Environmental Management (this issue).

Luo, T., 1996. Patterns of net primary productivity for Chinese majorforest types and its mathematical models. Ph.D. Dissertation. Commission for Instegrated Survey of Natural Resources, Chinese Academy of Sciences.

Menzies, N.K., 1996. Forestry, in science and civilization in China. In: Needham, J. (Ed.), Biology and Biological Technology, vol. 6. Cambridge University Press, New York, pp. 547–565.

Potter, C.S., Randerson, J.T., et al., 1993. Terrestrial ecosystem production: a process model based global satellite and surface data. Global Biogeochemistry Cycles 7, 811–841.

Price, D.T., McKenney, D.W., Nalderc, I.A., et al., 2000. A comparison of two statistical methods for spatial interpolation of Canadian Monthly Mean Climate Data Agricultural and Forest Meteorology. Agricultural and Forest Meteorology 101, 81–94.

Prince, S.D., Goward, S.N., 1995. Global primary production: a remote sensing approach. Journal of Biogeography 22, 815–835.

Ruimy, A., Saugier, B., Dedieu, G., 1999. Methodology for the estimation of terrestrial net primary production from remotely sensed data. Journal of Geophysics Research 99D3, 5263–5383.

Running, S.W., Nemani, R.R., Peterson, D.L., et al., 1989. Mapping regional forest evapotranspiration and photosynthesis by coupling satellite data with ecosystem simulation. Ecology 70, 1090–1101.

Sellers, P.J., Randall, D.A., Collatz, G.J., et al., 1996. A revised land surface parameterization (SiB2) for atmospheric GCMs. Part I: model formulation. Journal of Climate 9, 676–705.

Zhou, W., Liu, G., Pan, J., Feng, X., 2005. Distribution of available soil water capacity in China. Journal of Geographical Science 15, 3–12.